JOURNAL OF THERMOPHYSICS AND HEAT TRANSFER
Vol. 7, No. 4, Oct.–Dec. 1993

Computation of Nonequilibrium Hypersonic Flowfields Around Hemisphere Cylinders

Eswar Josyula* and Joseph S. Shang†
Wright Laboratory, Wright-Patterson Air Force Base, Ohio 45433

Hypersonic flows past hemisphere cylinders at zero incidence in chemical and thermal nonequilibrium are investigated for a range of Mach numbers from 10 to 18. The numerical code shows excellent comparison for surface pressure and heat transfer prediction with recent experiments conducted in a shock tunnel. The numerical code also compares well for stagnation point heat flux predictions at altitudes of 22 and 37 km with a set of earlier experiments. Numerical solutions with the vibrational equilibrium model are compared with those of multitemperature nonequilibrium. The stagnation point heat transfer is 10–23% higher for the nonequilibrium solutions in the Mach number range of 12–18. The importance of a multitemperature model for accurate prediction of stagnation properties, particularly the heat transfer, is noted. The variation in computed shock-standoff distance substantiates that the Mach number independence principle applicable to ideal gases does not hold for dissociating flows. Over the range of Mach numbers, the noticeable influence of vibrational relaxation on the temperature distributions and mass concentrations in the vicinity of shocks is shown in the present study.

Nomenclature

a = speed of sound
C_p = specific heat at constant pressure
C_v = specific heat at constant volume
c_i = mass fraction of species concentration, ρ_i/ρ
D_{ij} = binary diffusion coefficient
DX = distance along stagnation streamline measured from stagnation point
e = energy per unit mass, $e_s + (u^2 + v^2)/2$
e^* = vibrational energy per unit mass, based on translational temperature
e_s = specific internal energy, $\int C_v\, dT + \Delta h_f^0$
e_{vib} = vibrational energy per unit mass
$\dot{e}_{vib}$ = vibrational energy production per unit mass
$\tilde{F}, \tilde{G}$ = inviscid flux vectors
h = enthalpy
J = Jacobian of the coordinate transformation
k = thermal conductivity of the gas mixture
Le = Lewis number, 1.4
M = Mach number, third body of collision
p = static pressure
$\dot{q}$ = heat flux
R = gas constant
Rey = Reynolds number based on nose radius
R_n = nose radius
T = translational temperature
T_v = vibrational temperature
$\boldsymbol{u}$ = vector of mass average velocity components, u and v in body-tangential and radial direction, respectively
$\boldsymbol{u}_i$ = vector of diffusion velocity components, $u_i + v_i$ in body-tangential and radial direction, respectively
$\boldsymbol{W}$ = vector of extrapolated variables
X_i = mole fraction of species i
x, r, θ = coordinates of governing equations
Δh_f^0 = heat of formation
δ = entropy correction parameter
$\tilde{\delta}$ = coefficient in the entropy correction parameter
Θ_v = characteristic temperature for vibration
θ_{min} = minimum angular grid spacing, deg
λ = eigenvalue
μ = viscosity coefficient
ξ, η = transformed body-oriented coordinates
ρ = density of mixture
$\bar{\tau}$ = stress tensor
τ_i = vibrational relaxation time for species i
τ_{ik} = Landau-Teller interspecies vibrational relaxation time
$\dot{\omega}$ = source term of species conservation equation

Subscripts
i = species
wall = wall condition
∞ = freestream condition

Presented as Paper 92-2874 at the AIAA 27th Thermophysics Conference, Nashville, TN, July 6–8, 1992; received Aug. 21, 1992; revision received Dec. 11, 1992; accepted for publication Jan. 5, 1993.

*Aerospace Engineer, Flight Dynamics Directorate. Member AIAA.
†Senior Scientist, Flight Dynamics Directorate. Associate Fellow AIAA.

Introduction

THE presence of a strong bow shock wave in hypersonic flow past a blunt forebody causes considerable difficulties for accurate numerical and experimental simulation of the flowfield in the stagnation region. The shock wave converts the high kinetic energy of the oncoming flow into the various internal energy modes, leading to significant chemical and thermal nonequilibrium[1] in the stagnation region.

Previous work of Josyula et al.[2–4] successfully simulated the hypersonic nonequilibrium flow past blunt bodies for a free-stream Mach number of 12 at 30-km altitude. The flow was assumed to be in thermal equilibrium, but in chemical non-equilibrium. Conditions were so chosen that the flow was at a state of a small departure from chemical equilibrium and the assumption of vibrational equilibrium was valid. The work of Refs. 2 and 3 used the explicit MacCormack scheme to solve the Navier-Stokes equations with chemical physics. The anomalous numerical bulge encountered in the stagnation region for flow past a blunt body was controlled by using an adaptive grid procedure.[2] The work of Ref. 4 used the Roe flux-difference split scheme to solve the inviscid part of the governing Navier-Stokes equations without grid adaptation. The anomalous numerical bulge was effectively controlled by the entropy correction parameter in the Roe scheme, resulting in smooth surface heat transfer profiles. Solutions compared well with classic theory and other computational results.

However, at higher Mach numbers and altitudes, the flow departs from thermal equilibrium and the energy exchange

into the various modes due to the vibrational excitation and relaxation becomes important. As the vibrational excitation and relaxation sequence progresses, excitation to higher and higher vibrational levels occurs until the molecule dissociates. So it becomes important to understand the collision-induced transition probabilities to the dissociation process and thermal activation. Above a temperature of 2500 K, the vibrational modes of the air mixture become excited and energy is exchanged in a ladder-climbing process, first the vibration-vibration exchange, then the vibration-translation exchange, thereafter, the molecules start to dissociate from the highly excited vibrational levels. The reaction rate for dissociation is not accurately determined by a single translational temperature.[5,6] The vibration-dissociation coupling models due to Park,[7] Marrone and Treanor,[8] and Jaffe,[9] which make use of separate translational and vibrational temperatures, are widely used. The vibration-dissociation model of Marrone and Treanor[8] is based on the harmonic oscillator model and its vibrational states having a Boltzmann distribution at the vibrational temperatures. At highly nonequilibrium conditions, the inaccuracy of this model has been shown by Sharma et al.[10] In the coupling suggested by Jaffe,[9] the influence of the chemistry on the vibrational energy relaxation is not considered. Flament[11] extended the approach of Jaffe[9] to couple the chemistry and vibrational relaxation, and concluded that the average mass recombination vibrational energy is far too high. For the present work, the vibration-dissociation coupling is modeled according to the empirical relationship proposed by Park.[10,12] This coupling model considers only the influence of vibration on the dissociation without explicitly modifying the vibrational energy relaxation equation. However, for each species, a rate controlling temperature is defined as an appropriate average of the translational and vibrational temperatures which is known to give correct phenomenological trends.[12] The translation-vibration energy exchange is considered by the theory of Landau and Teller[13] and the interspecies relaxation times given by the expression of Millikan and White.[14]

In the literature, code validation with experiments for nonequilibrium hypersonic flow has mostly focused on the qualitative features of the flowfield.[6,15] Comparing the computational prediction of surface heat transfer and pressure with classic results (both theoretical and experimental) and recent experimental results is one of the objectives of this work. The effects of conditions at altitudes of 22 and 37 km for Mach numbers ranging from 12 to 18 are discussed in the present work. This article is also concerned with the difference between the assumption of vibrational equilibrium and the vibrational nonequilibrium phenomenon at shock temperatures below 14,000 K.

The objective of the present work is to model the Navier-Stokes equations with chemical and thermal nonequilibrium using the Roe flux-difference split scheme, and to validate the results with experiments and to understand the influence of vibrational relaxation for a range of Mach numbers.

Analysis

Governing Equations

The global conservation equations with chemical and thermal nonequilibrium in mass average velocity form are as shown below:

$$\frac{\partial}{\partial t}(\rho_i) + \nabla\cdot[\rho_i(\boldsymbol{u} + \boldsymbol{u}_i)] = \dot{\omega}_i \tag{1}$$

$$\frac{\partial}{\partial t}(\rho \boldsymbol{u}) + \nabla\cdot(\rho \boldsymbol{u}\boldsymbol{u} + \bar{\tau}) = 0 \tag{2}$$

$$\frac{\partial}{\partial t}(\rho_i e_{\text{vib}_i}) + \nabla\cdot[\rho_i e_{\text{vib}_i}(\boldsymbol{u} + \boldsymbol{u}_i) + \dot{q}_{\text{vib}_i}] = \rho_i \dot{e}_{\text{vib}_i} + e_{\text{vib}_i}\dot{\omega}_i \tag{3}$$

$$\frac{\partial}{\partial t}(\rho e) + \nabla\cdot\left[\rho e\boldsymbol{u} - \dot{q}_{\text{trans}} - \sum_i \dot{q}_{\text{vib}_i} + \sum_i (\rho_i h_i \boldsymbol{u}_i) - \boldsymbol{u}\cdot\bar{\tau}\right] = 0 \tag{4}$$

For the cases where vibrational energy is considered in equilibrium with the translational temperature, Eq. (3) (the vibrational energy conservation equation) is not required. Instead, the specific internal vibrational energy is computed using the expression for the simple harmonic oscillator. The expression for the equilibrium vibrational C_v for diatomic molecules is given as[16]

$$C_{v_{\text{vib}}} = R\left(\frac{\Theta_v}{T}\right)^2 \frac{e_s^{(\Theta_v/T)}}{[e_s^{(\Theta_v/T)} - 1]^2} \tag{5}$$

Upper limit of temperature for the present analysis is restricted to 14,000 K, and the maximum altitude considered is 37 km. Since the primary purpose of this article is to study dissociating flows with vibrational nonequilibrium, the physics of ionization and radiation of atomic species are neglected. The translational-vibrational coupling shown in Eq. (3), is modeled according to the Landau-Teller[13,16] form, which assumes that the vibrational level changes by one quantum level at a time:

$$\dot{e}_{\text{vib}} = \rho_i[(e^*_{\text{vib}_i} - e_{\text{vib}_i})/\tau_i] \tag{6}$$

The relaxation time is computed as[17]

$$\tau_i = \frac{\sum_i X_i}{\sum_i X_i/\tau_{ik}} \tag{7}$$

τ_{ik} are computed using the expression developed by Millikan and White.[14] The vibration-vibration coupling has been neglected in the present analysis. The vibration-dissociation coupling for the diatomic species is achieved by the two-temperature model suggested by Park[7,10]

$$T_d = T^{0.7}T_v^{0.3} \tag{8}$$

where T_d is the rate-controlling dissociation temperature. For a shock-layer temperature less than 14,000 K, the primary species are O_2, O, N_2, N, and NO. The significant chemical reactions between these species, excluding ionization, are[5]

$$\begin{aligned} N_2 + M &\rightleftharpoons 2N + M \\ O_2 + M &\rightleftharpoons 2O + M \\ NO + M &\rightleftharpoons N + O + M \\ N_2 + O &\rightleftharpoons NO + N \\ NO + O &\rightleftharpoons O_2 + N \end{aligned} \tag{9}$$

The chemical source terms are derived from the law of mass action,[16] considering the five possible reactions occurring between the species of the air mixture. The reaction rates and equilibrium constants are taken from the work of Park.[5] A separate species-conservation equation [Eq. (1)] is solved for each species, O_2, O, N_2, N, and NO. For the vibrational energy conservation equation [Eq. (3)], a separate equation is solved for each of the diatomic species, O_2, N_2, and NO. The ratio of specific heats γ is given by $\gamma = 1 + \bar{R}/C_v$, where $\bar{R} = \Sigma\, \rho_i R_i$ and $C_v = \Sigma\, \rho_i C_{v_i}$.

The species viscosity is computed from the curve fits of Blottner et al.[18] which are valid up to temperatures of 10,000

Table 1 Details of nominal flow conditions used to simulate experiments in shock tunnel

Mach no.	Re_∞	T_∞, K	p_∞, Pa	T_{wall}, K	R_n, m	Wall condition
9.8	3,842	450	0.0023	555.5	0.0127	Noncatalytic
9.8	7,684	450	0.0023	555.5	0.0254	Noncatalytic
9.8	15,371	450	0.0023	555.5	0.0508	Catalytic and noncatalytic

K. The species thermal conductivity is calculated from Eucken's relation[16]

$$k_i = \mu_i(\tfrac{5}{2}Cv_{\text{trans}_i} + Cv_{\text{int}_i}) \tag{10}$$

where Cv_{trans} is the specific heat for the translational energy mode, and Cv_{int} represents the specific heat associated with the internal modes, namely, the rotational and vibrational energy. The viscosity and thermal conductivity of the mixture are computed by the Wilke's semiempirical mixing rule.[19]

In the present analysis only the ordinary diffusion generated by species concentration is considered. The diffusion mass flux is according to the Fick's first law of diffusion[20]

$$\rho_i u_i = -\rho D_{ij} \nabla c_i \tag{11}$$

where D_{ij} is calculated by assuming a constant Lewis number of 1.4. The Lewis number is

$$Le = (\rho D_{ij} C_p / k) \tag{12}$$

Numerical Procedure

The Roe approximate Riemann solver is implemented in finite volume formulation by computing the cell interface flux as a summation over wave speeds. For an $i + \frac{1}{2}$ face[21]

$$\tilde{F}_{i+1/2} = \frac{1}{2}(\tilde{F}_l + \tilde{F}_r) - \frac{1}{2}\sum \tilde{a}_i |\tilde{\lambda}_i| \tilde{E}_i \tag{13}$$

where the subscripts l and r represent evaluation at the left and right of interface $i + \frac{1}{2}$, respectively. $\tilde{a}_i$ is the wave strength corresponding to the ith eigenvalue, and $\tilde{\lambda}_i$ and $\tilde{E}_i$ are the associated eigenvalue and eigenvector, respectively. Formal second-order spatial accuracy is obtained by employing the MUSCL approach[22] in conjunction with the "minmod" limiter[23] to reduce the solution to first-order accuracy in the vicinity of strong shock waves. The equations for the MUSCL approach are

$$W^r_{i+1/2} = W_{i+1} - \tfrac{1}{2}\tilde{\Delta}_{i+3/2} \tag{14}$$

$$W^l_{i+1/2} = W_i + \tfrac{1}{2}\tilde{\Delta}_{i+1/2} \tag{15}$$

where

$$\tilde{\Delta}_{i+1/2} = \text{minmod}(\Delta_{i+1/2}, \Delta_{i-1/2}) \tag{16}$$

and $\Delta_{i+1/2} = W^r - W^l$. The vector $W = \{\rho_i, u, v, p\}$ is extrapolated to each interface to yield the vector of conserved variables $\tilde{U}$. The interface fluxes, Roe averages for u, v, ρ_i, h, and speed of sound of the Roe scheme are implemented as given in the work of Walters et al.[24]

The entropy condition is enforced by appropriately cutting off the eigenvalues

$$\tilde{\lambda} = \begin{cases} \tilde{\lambda} & \tilde{\lambda} \geq \delta \\ \dfrac{\tilde{\lambda}^2 + \delta^2}{2\delta} & \tilde{\lambda} < \delta \end{cases} \tag{17}$$

In the treatment of the entropy cutoff, the isotropic formula

$$\delta = \tilde{\delta} J^{-1}[|u \cdot \nabla \xi| + |u \cdot \nabla \eta| + (a/2)(|\nabla \xi| + |\nabla \eta|)] \tag{18}$$

is utilized in the η (body-normal) direction, while the anisotropic formula

$$\delta = \tilde{\delta} J^{-1}[1 + (\lambda^{(\eta)}/\lambda^{(\xi)})^{2/3}] \tag{19}$$

where $\lambda^{(k)} = |u \cdot \nabla k| + a|\nabla k|$, $k = \xi, \eta$ is employed in the ξ (body-tangential) direction. In these equations the cutoff parameter $\tilde{\delta}$ is given by the range $0.01 < \tilde{\delta} < 0.5$.

The viscous terms are evaluated using central differencing. An explicit predictor-corrector method is used to advance the solution in time. This approach was discussed for the flux-splitting option by MacCormack in Ref. 25.

Conditions of Numerical Simulation

The computational results are compared with recent experimental observations reported by Barr et al.[26] and Cassady et al.[27] for surface pressure and surface heat transfer distributions. A shock tunnel was used to produce the required hypersonic flow conditions to effect chemical and thermal nonequilibrium flow past blunt bodies. Three hemisphere-cylinders with different radii for the hemisphere were chosen for blunt bodies. The radii for the three bodies, referred to as model 1, model 2, and model 3, are 0.0127, 0.0254, and 0.0508 m, respectively. The conditions used for the numerical simulation of flows past blunt bodies to compare with experiments in the shock tunnel are given in Table 1. The wall heat flux was determined by two methods: 1) using a coaxial thermocouple gauge, and 2) using a thin film gauge. The blunt bodies were made of stainless steel. When the thin-film gauge was used, care was taken in overcoating the gauges with mother of pearl to minimize the wall catalycity. Wall catalytic effects were allowed in the measurement of heat transfer when the thermocouple gauge was used for measurement. The computations are also compared with the shock tube measurements of stagnation point heat flux for flow past blunt bodies from the work of Rose et al.[28] In this work, the flow conditions produced at the stagnation point of a hemisphere-cylinder model in the shock tube are used to simulate the flight situation. The stagnation enthalpy for the blunt body in the shock tube was related to the stagnation enthalpy at flight conditions. This results in the expression, $V_f = \sqrt{(2V_sV_g)}$. Here, V_f is the flight velocity; V_s and V_g are the velocities of the moving shock wave and gas, respectively, in the shock tube. In this manner, stagnation point heat flux measurements of the shock-tube were correlated with a wide range of flight speeds at altitudes of 22 and 37 km in the work of Rose et al.[28] Calorimeter gauges were used on hemisphere cylinders made of Pyrex®. Care was taken in minimizing wall-catalytic effects in the prediction of surface heat transfer. Similar experiments were conducted by Polyakov[29] for a limited range of flow conditions showing excellent agreement with the work of Rose et al.[28] and Fay et al.[30] From the work of Rose et al.,[28] a limited set of flow conditions was selected for numerical simulation in the present study. Conditions at free-stream Mach numbers of 12, 14, 16, and 18, at altitudes of 22 and 37 km are considered in the present investigation. Computations were conducted for cases of both vibrational equilibrium and nonequilibrium. Flow conditions are given in Table 2.

Grid resolution study was performed to determine the number of points required to achieve grid-independent solutions for a flow in chemical nonequilibrium with the current nu-

Table 2 Details of flow conditions used to simulate experiments in shock tube

Mach no.	Re_∞	T_∞, K	T_{wall}, K	R_n, m	Alt, km
12	103,329	218	555.5	0.0066	22
12	8,560	252	555.5	0.0066	37
14	120,550	218	555.5	0.0066	22
14	9,987	252	555.5	0.0066	37
16	137,770	218	555.5	0.0066	22
16	11,413	252	555.5	0.0066	37
18	154,990	218	555.5	0.0066	22
18	12,840	252	555.5	0.0066	37

Note: Noncatalytic wall boundary condition is used for all cases.

Table 3 Details of grids considered in this study

Mach no.	Δn	θ_{min}	R_n, m	Body length, m
9.8	3.175E-6	1.950	0.0127	0.1143
9.8	2.54E-6	1.950	0.0254	0.2032
9.8	2.54E-6	1.950	0.0508	0.4064
12, 14, 16, 18	0.79E-6	0.162	0.0066	0.0132

Δn = Effective (half-cell) minimum spacing, m.
θ_{min} = Minimum angular spacing, deg.
Note: All grids have 40 points in body-tangential direction, and 50 points in radial direction.

merical algorithm, in the earlier work of Josyula et al.[4] In the present study, a mesh system of 40 nodes in the body-tangential direction and 50 nodes in the body-normal direction was used for all cases. The first grid spacing normal to the body at the stagnation point is crucial in the prediction of surface heat transfer, as also observed by Hoffman et al.[31] This spacing is required to satisfy a certain minimum for predicting grid-independent results in the stagnation region. The minimum spacing and other grid details used in the present study are given in Table 3.

The computation was performed in local time-stepping mode with a Courant-Friedrich-Lewy (CFL) number of 0.9. In order to overcome the stiffness due to the source terms a lower CFL was used during the transients. Iterative convergence was monitored by examining the surface heat transfer over several characteristic times based on the minimum time-step size. Convergence is achieved when the change in surface heat transfer does not change more than 1% between two consecutive solutions of one time unit apart. The L2 norm of the residual was also monitored. A criterion of convergence is met after the normalized residual drops more than eight orders of magnitude. To satisfy the convergence criterion for obtaining a steady-state solution, a maximum of 20,000 time steps were required when the initial conditions were specified as uniform flow. The data processing rate (DPR) for the axisymmetric solution of the Navier-Stokes equations with five species in vibrational equilibrium is 2.68×10^{-4} cpu-s/pt/iter, and that with vibrational nonequilibrium is 3.38×10^{-4} cpu-s/pt/iter on Cray XMP/216 computer.

Boundary Conditions

The upstream and far-field boundary conditions are prescribed as the undisturbed freestream values. At the downstream boundary, the no-change condition is imposed for the predominantly supersonic flowfield. On the body surface, the nonslip condition for velocity components, an isothermal wall, and the approximation of zero normal pressure gradient are enforced. The species are set for a noncatalytic wall boundary condition for all cases. In addition, model 3 simulation of the shock tunnel is set to fully catalytic boundary condition to conform to conditions of the experiment.[32] The finite volume formulation of the present work allows fluxes at the singular line of symmetry to be set to zero because the control volume surface at the axis of symmetry merges to a point.

Discussion of Results

The results are presented in two sections. In the first section, computations are compared with experimental data on flow past hemisphere cylinder bodies. The data is collected by producing hypersonic flow conditions in a shock tunnel.[26,27] Flow conditions are given in Table 1. In the second section, computations are compared with experiments[28] on flow past a blunt body for a range of Mach numbers corresponding to two different altitudes. Flow conditions are given in Table 2. The physics is discussed for flows at different altitudes and with the vibrational state considered to be in equilibrium and nonequilibrium.

Comparison with Data Having Nose Radius Variation

In this section, the comparison of surface pressure and heat transfer is made with data for nonequilibrium flow past three blunt bodies of different radii, referred to as model 1, model 2, and model 3. The temperature distribution along the stagnation streamline is also shown for the three bodies, depicting the nonequilibrium phenomenon.

Figure 1 compares the surface pressure distribution for three hemisphere cylinder bodies with different nose radii and cylinder lengths. The locations for pressure measurement are along the afterbody for all three models. The comparison for model 1 is excellent and is within experimental scatter for models 2 and 3. The surface heat transfer distribution for the three models is shown in Fig. 2. The comparison is shown for two different types of measurement of heat flux, thermocouple gauge, and thin film gauge. The agreement of present computations and data is within the experimental scatter of both the gauges for the afterbody.

The surface heat transfer distribution in the stagnation region is shown in Fig. 3. The models are made of stainless steel allowing wall-catalytic effects for inclusion in the prediction of heat transfer. It may be noted that a thin film gauge was used for the measurement for models 1 and 2, and the wall catalycity was minimized by covering the gauges with mother of pearl. However, a thermocouple gauge was used for the heat transfer measurement for model 3 allowing for catalytic effects. The material of the gauge was so selected that its thermal properties were similar to that of the surface. Hence, the wall boundary conditions specified for the numerical computation to conform to experiments are as follows: noncatalytic wall assumption for models 1 and 2, and a fully catalytic wall for model 3. The noncatalytic wall boundary condition was also used for model 3 for the sake of comparison. The calculated stagnation point heat transfer is within the experimental scatter for models 1 and 2. The computation underpredicts the experiment by 10% for model 3. Similar discrepancy is noticed in the results of numerical simulation reported by Barr.[26] Only one measurement was taken for model 3 for practical considerations, hence, the uncertainty is reported as zero.[26] From Fig. 3, we can also note that the increase in heat transfer for the fully catalytic wall is predicted numerically to be 62% above the noncatalytic wall. Finite catalytic rates, however, will limit the surface heat transfer predictions to within this difference. The experimental uncertainty in heat transfer due to catalytic conditions of the gauges is discussed in Refs. 32 and 33. Figure 3 also shows the heat transfer in the stagnation region along the surface of the body decreasing with an increase in radius, indicating the importance of the temperature gradient near the surface (see Fig. 4). It is noted that the time taken for a fluid particle to travel from the stagnation point to the shoulder of the nose is longer for the body with greater nose-radius.

The predicted temperature distribution along the stagnation streamline for the three models is shown in Fig. 4. The peak temperatures are nearly the same for all three models, but the shock-standoff is proportional to the radius of the hemisphere. It is also noticed that the temperature gradient near the surface is steeper with decreasing radius as discussed for Fig. 3.

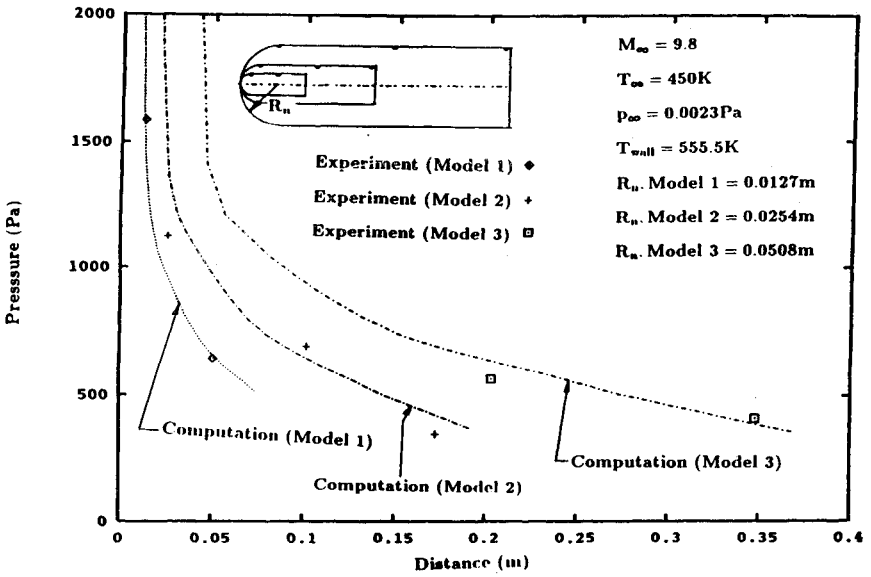

Fig. 1 Comparison of surface pressure distribution with shock-tunnel experiments for three different-sized models.

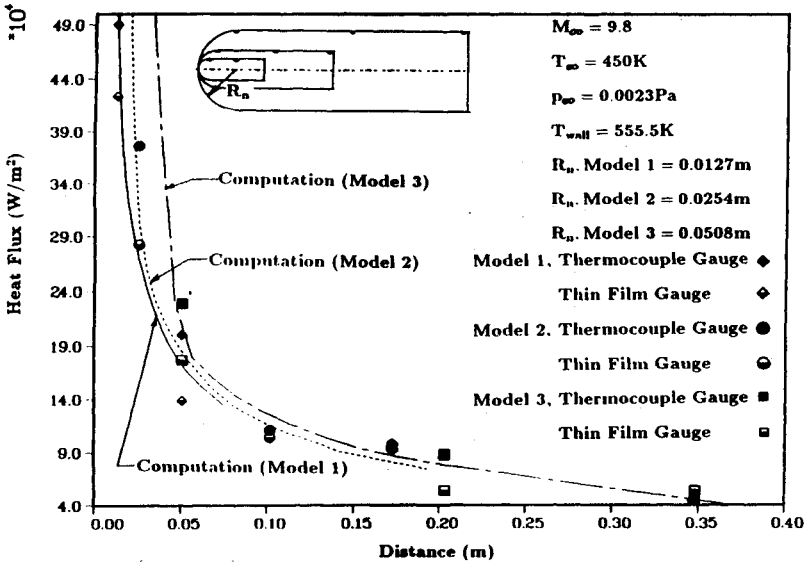

Fig. 2 Comparison of surface heat transfer distribution with shock-tunnel experiments for three different-sized models.

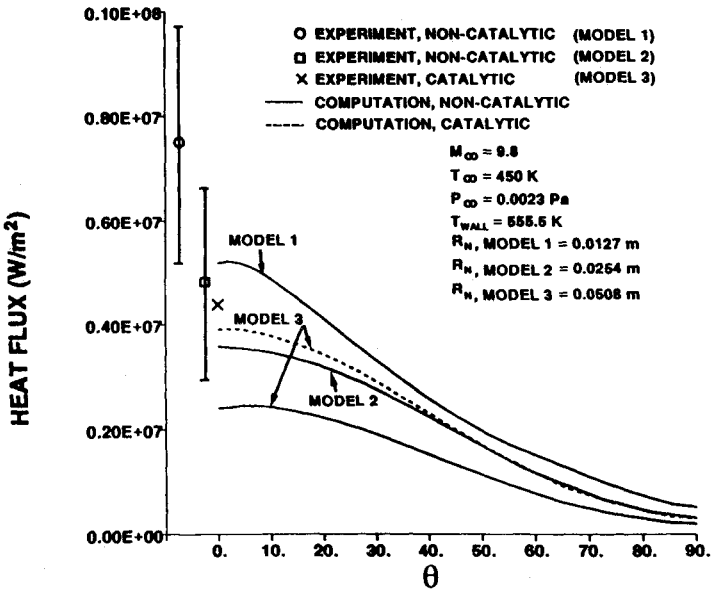

Fig. 3 Surface heat transfer distribution for three different-sized models.

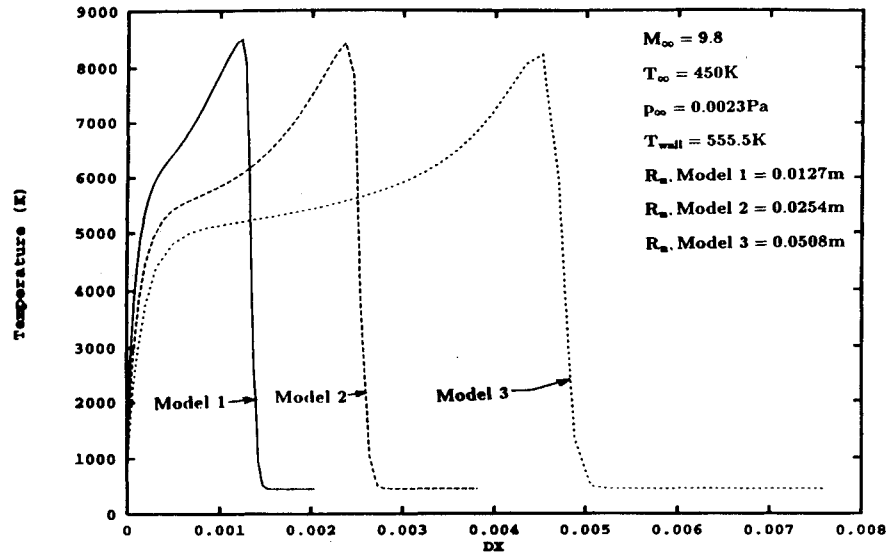

Fig. 4 Temperature distribution along stagnation streamline for three different-sized models.

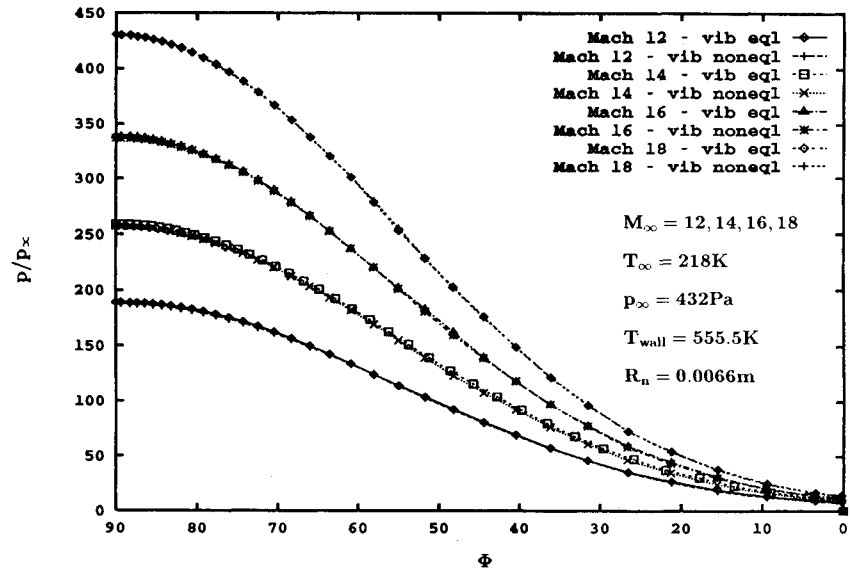

Fig. 5 Comparison of surface pressure distribution at different Mach numbers for vibrational equilibrium and vibrational nonequilibrium.

Comparison with Data Having Variation in Altitude and Mach Numbers

In this section, numerical results are discussed for the Mach number range of 12–18 for altitudes of 22 and 37 km. Stagnation point heat transfer is compared to data, and the physics is discussed for nonequilibrium flows with reference to classic hypersonic flow theory. Reference 28 gives details of experiments. See Table 2 for details of flow conditions used for numerical simulation.

Figure 5 shows the predicted surface pressure distribution at different Mach numbers for both cases of vibrational equilibrium and nonequilibrium. The distribution for both the cases are identical, substantiating known theory that there is no contribution of vibrational excitation to the pressure. However, as expected, the pressure increases with increase in Mach number. The stagnation point heat transfer at different flight speeds is compared with the theoretical prediction of Lees[28] in Fig. 6. The vibrational temperature is assumed to be in equilibrium with the translational temperature. The comparison of the present computation with the theoretical calculation is excellent for all Mach numbers investigated.

The stagnation point heat transfer is compared with experiments of Rose et al.,[28] in Fig. 7, at altitudes of 22 and 37 km at different flight speeds. The present computation follows the trends of the experiment, but uniformly underpredicts it at both altitudes. The underprediction of the present computation is between 20–30% below the experimental data. It is also noticed that the heat transfer is lower for the higher altitude cases, and the difference between results of different altitudes increases with increase in flight speed. The decrease in stagnation point heat flux at the higher altitude cases is caused by the higher degree of dissociation which lowers the temperature near the surface, thus lowering the heat transfer. It is also noted that for both altitudes shown in the figure, at the minimum and maximum flight speeds (ratio of square of velocity is 2.25), the ratio of stagnation point heat transfer is about 3.2, substantiating the classic theory of the high influence of kinetic energy.

The surface heat transfer distributions at different flow speeds for the cases of vibrational state in equilibrium and nonequilibrium are shown in Fig. 8. The increase in heat transfer for the case of vibrational nonequilibrium is nearly 10% for a Mach number of 12. The difference in heat transfer increases for the case of Mach 14. The difference in heat transfer at the two vibrational states however, stays nearly constant for Mach 16 and 18. The maximum increase in heat transfer for the vibrational nonequilibrium case is nearly 23% for Mach

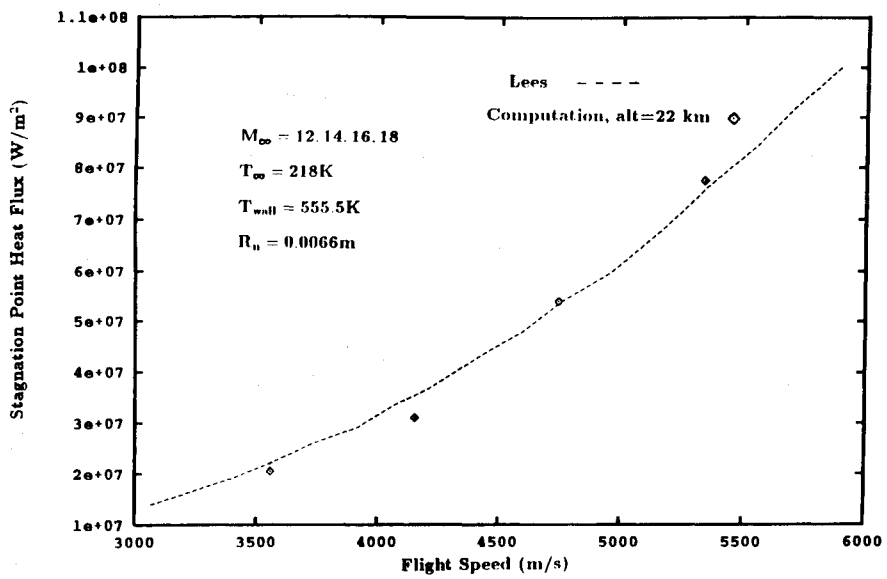

Fig. 6 Comparison of stagnation point heat flux with calculation of Lees[28] at different flight speeds.

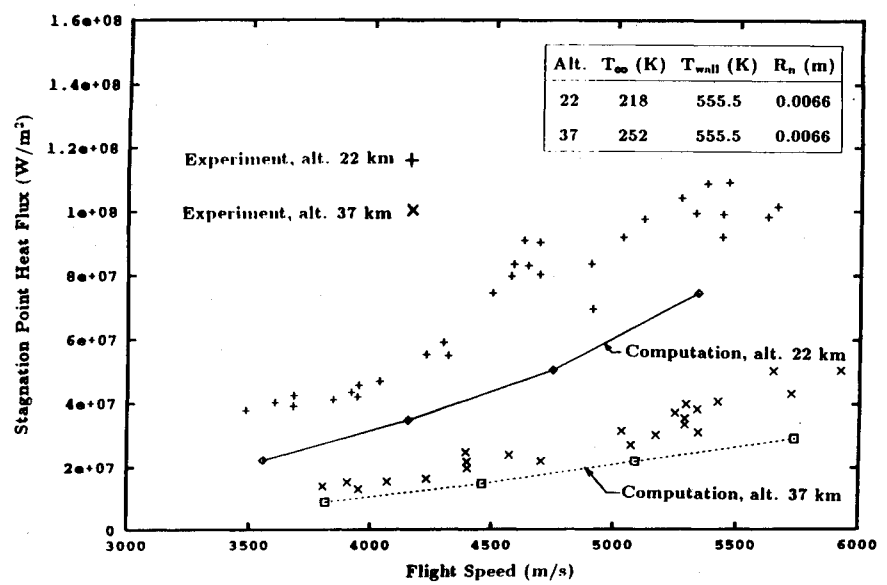

Fig. 7 Comparison of stagnation point heat flux with experiments at different flight speeds and altitudes.

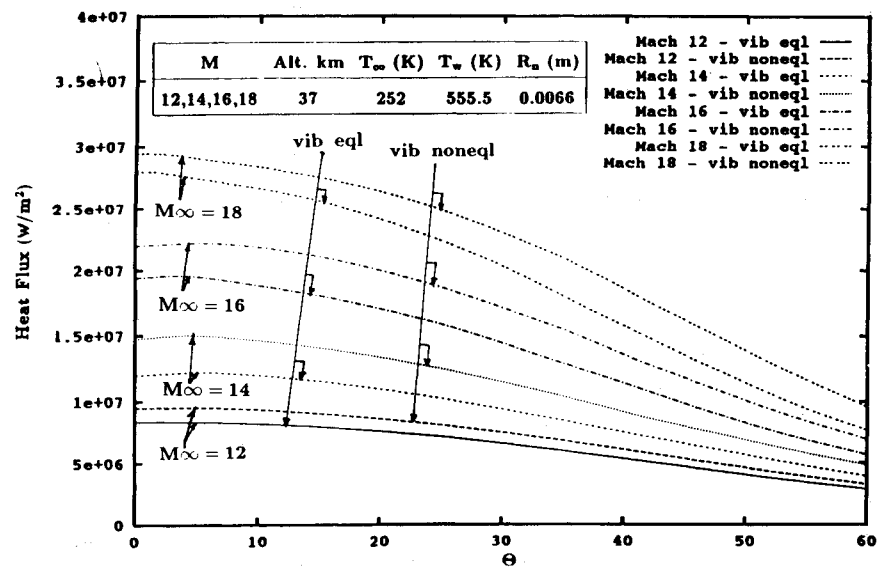

Fig. 8 Comparison of surface heat transfer distribution for different Mach numbers for vibrational equilibrium and vibrational nonequilibrium.

18. This suggests the importance of the phenomenon of vibrational relaxation on the prediction of the surface heat transfer distribution.

Figure 9 shows the translational temperature distribution along the stagnation streamline for the case of vibrational state in equilibrium and in nonequilibrium at Mach 12 and 18. For both Mach numbers it can be seen that the peak temperatures are lower and the shock-standoff distance is smaller for the case of the vibrational state in equilibrium. This is a result of the incorrect representation of vibrational temperature due to the assumption of the vibrational mode being in equilibrium with the translational mode. For the case of the vibrational state in equilibrium, the higher vibrational temperature leads to higher dissociation, and therefore, the lowering of the translational temperature.

The variations of translational temperature along the stagnation streamline for Mach 12 and 18 at altitudes of 22 and 37 km are given in Fig. 10 for flows in vibrational nonequilibrium. The ambient conditions at both altitudes are enhanced by the strong compression shock at these high Mach numbers. It is due to this reason that differences in temperature distributions and shock-standoff distances exist at both altitudes. The highest temperature, and consequently, the highest dissociation, occurs for the case of Mach 18 at 37-km altitude.

Figure 11 is a depiction of shock-standoff distances at different Mach numbers and different altitudes for cases of both equilibrium and nonequilibrium vibrational state. The reasons for the difference in shock-standoff distances are as previously mentioned for Figs. 9 and 10. For the cases of dissociating gas, it is interesting to note that for increasing Mach numbers, the shock-standoff distance keeps getting lower, which is different from the ideal gas behavior. The ideal gas shock-standoff distance reaches an asymptote at about 0.009 m and becomes Mach number-independent under these conditions, according to classic hypersonic theory.[34]

Since there is a greater degree of dissociation at the high-altitude case, the rest of the results presented are for the conditions at 37-km altitude for the gas in chemical and vibrational nonequilibrium. Figure 12 shows the variation of vibrational temperature of O_2 and translational temperature along the stagnation streamline at Mach numers of 12, 14,

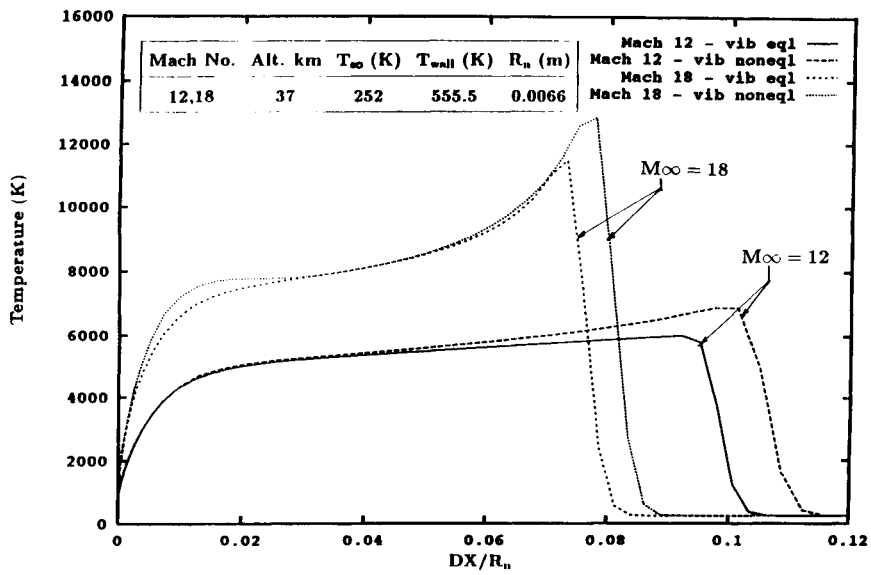

Fig. 9 Comparison of temperature distribution along stagnation streamline for different Mach numbers for vibrational equilibrium and vibrational nonequilibrium.

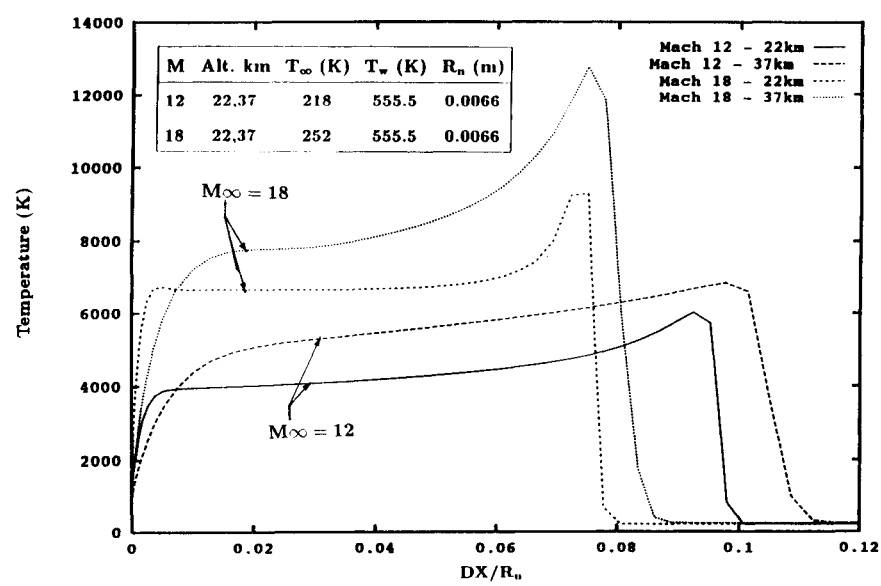

Fig. 10 Comparison of translational temperature distribution along stagnation streamline for different Mach numbers and altitudes.

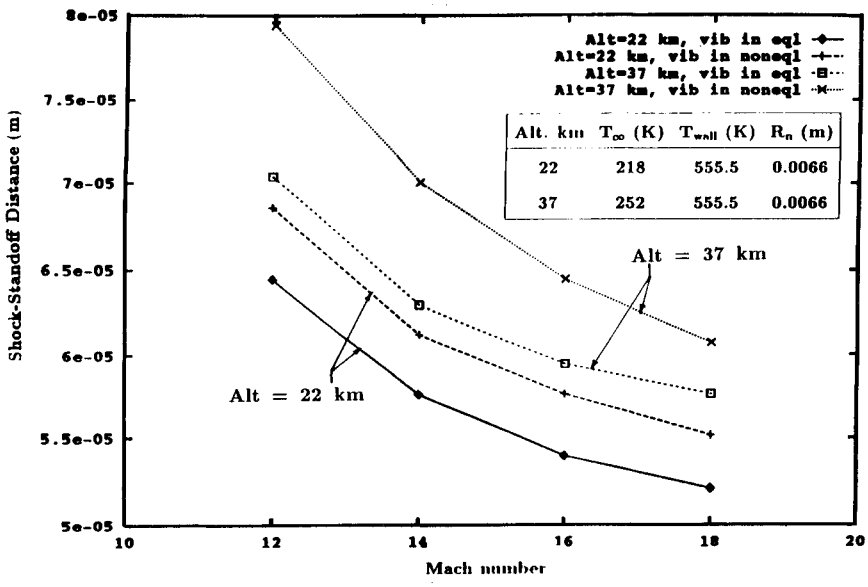

Fig. 11 Comparison of shock-standoff distance at different Mach numbers and altitudes.

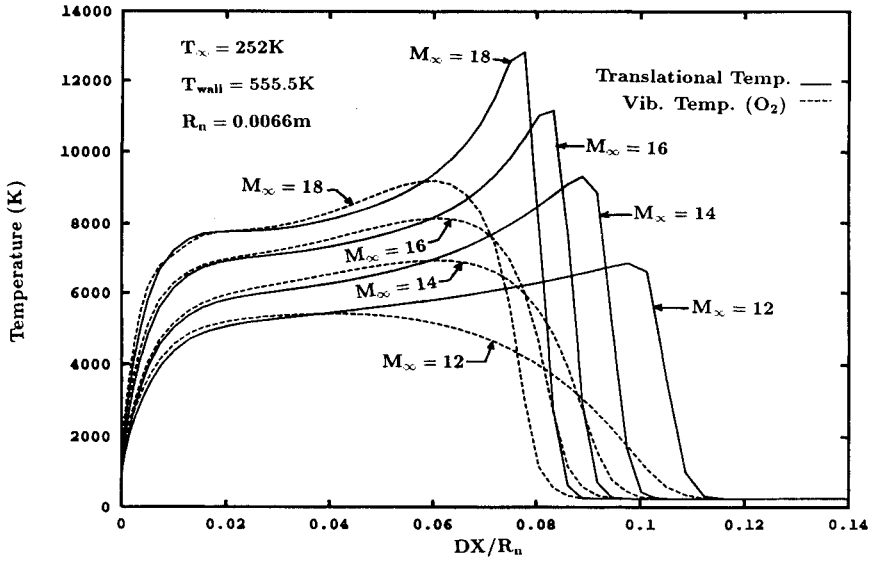

Fig. 12 Comparison of vibrational temperature of O_2 and translational temperature along stagnation streamline at different Mach numbers.

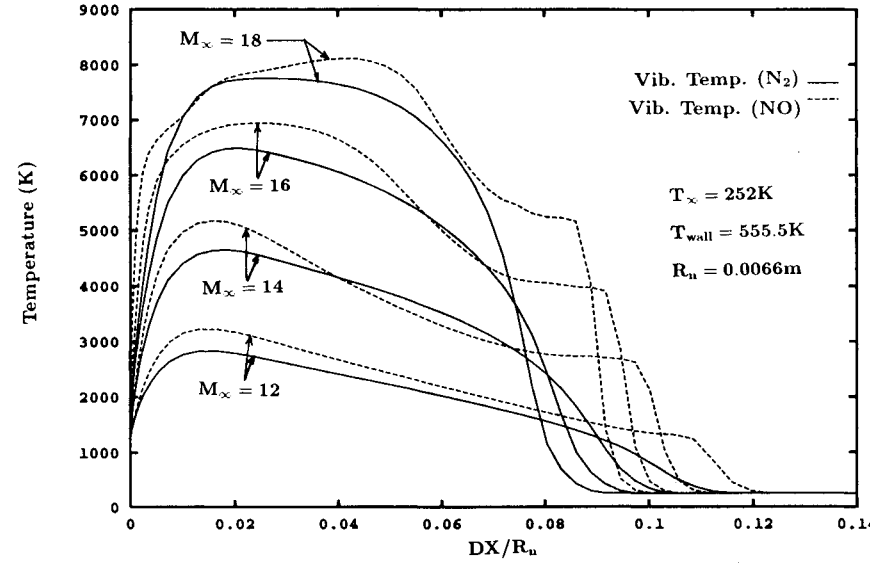

Fig. 13 Comparison of vibrational temperature of N_2 and NO along stagnation streamline at different Mach numbers.

16, and 18. Variations in translational temperature for Mach 12 and 18 have been discussed earlier in Figs. 9 and 10. The vibrational temperatures at different Mach numbers for molecular nitrogen and nitric oxide is given in Fig. 13. The peak translational temperature reached immediately downstream of the bow shock wave is the highest for the Mach 18 case. The translational temperature gradient is the highest near the body for the case of the Mach 18. The shock-standoff distance is the smallest for the Mach 18 case, suggesting higher degree of dissociation compared to other Mach numbers. It may be noted that the Mach number independence principle does not apply to gases departing from ideal gas behavior. It is also seen that the vibrational relaxation time for molecular oxygen, nitrogen, and nitric oxide in the postshock region is greatest for Mach 12 and the lowest for Mach 18, caused by higher density in the shock layer which enhances the collisional energy transfer mechanisms. The peak temperature, however, is highest for Mach 18 and lowest for Mach 12, as expected.

Figure 14 depicts the translational and vibrational temperature variations along the stagnation streamline for the case of Mach 18. The nonequilibrium behavior of the vibrational energy mode can be seen from the temperature profiles near the shock region. It can be seen from the variation of the vibrational temperatures in the vicinity of the shock wave that the vibrational relaxation time for O_2 is the lowest. From the present numerical result, the vibrational degree of freedom (DOF) of NO is the most easily exicited among all diatomic components of the air mixture considered in the present study. The vibrational temperature of NO reaches about 6000 K before the translational temperature increases from its free-stream value. It is caused by the relatively high diffusion velocity of species NO in the vicinity of shock wave. The relatively high vibrational temperature can be understood by examination of the relative elementary reaction rate coefficients and the low heat of formation of NO. This peculiar phenomenon was also observed in an earlier effort.[35] It is indicative of the importance of vibration-dissociation coupling at temperatures less than 6000 K in the vicinity of the shock wave.

Figures 15–17 show the mass concentrations of atomic and molecular oxygen and nitrogen and nitric oxide for different Mach numbers. From these figures, it can be clearly seen that the relaxation time in the vicinity of the shock wave is highest for Mach 12 and lowest for Mach 18. The concentration of O_2 on the surface is less than 3% for Mach 14, 16, and 18, but more than 10% still exists for the case of Mach 12. The

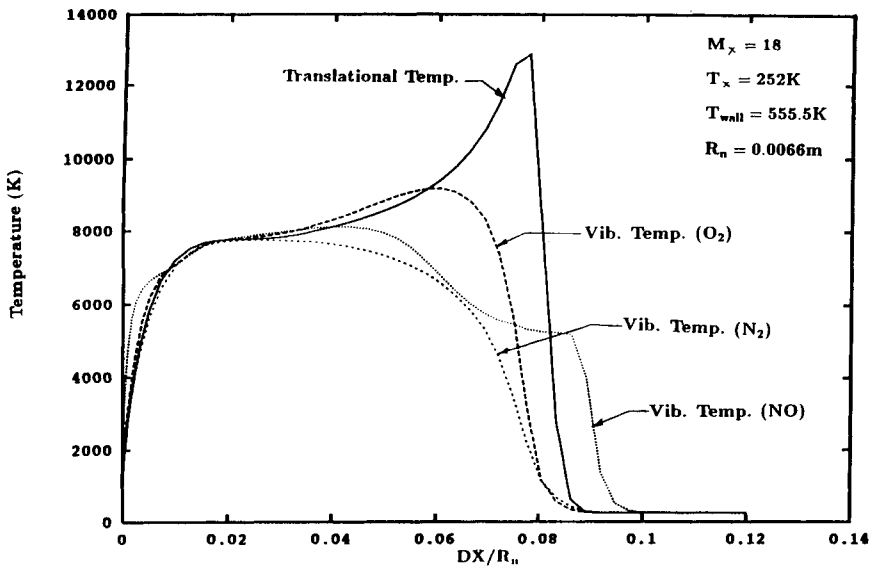

Fig. 14 Comparison of translational and vibrational temperatures along stagnation streamline.

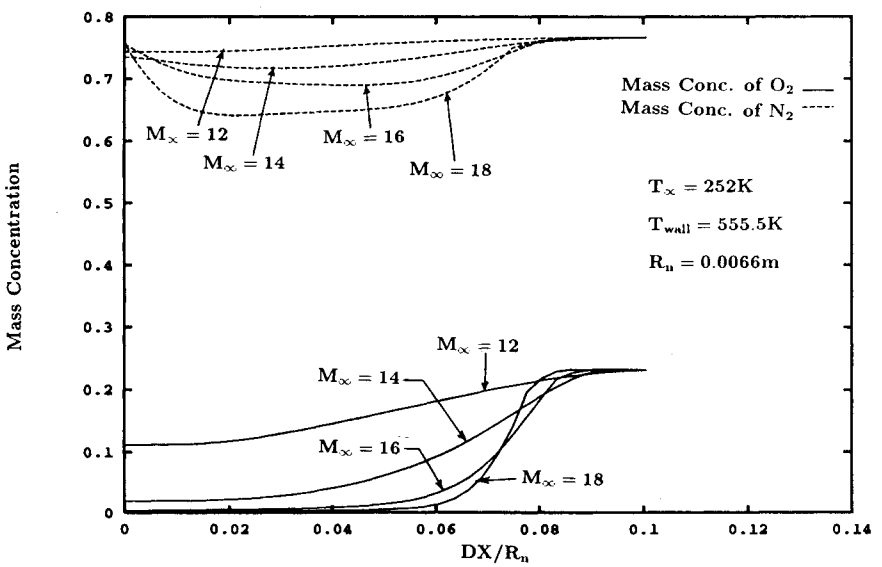

Fig. 15 Comparison of mass concentration of O_2 and N_2 along stagnation streamline at different Mach numbers.

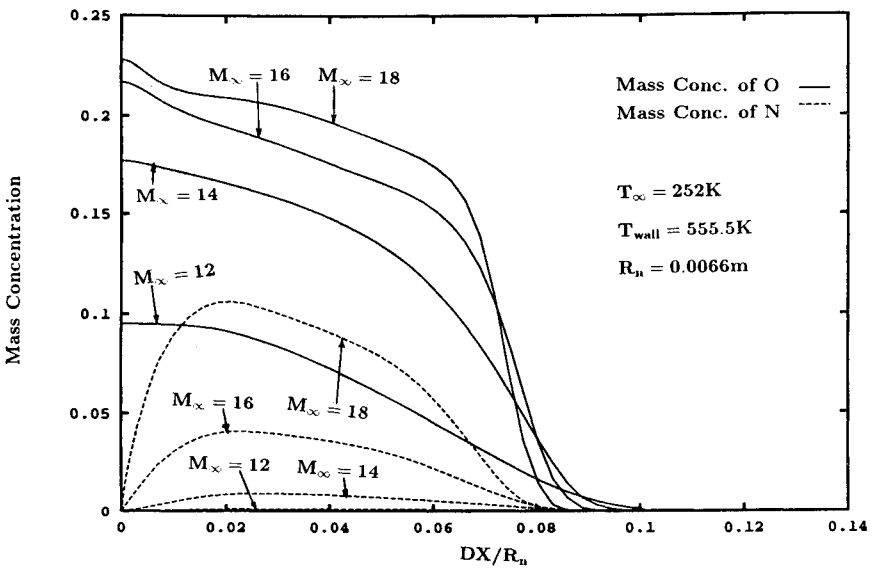

Fig. 16 Comparison of mass concentration of O and N along stagnation streamline at different Mach numbers.

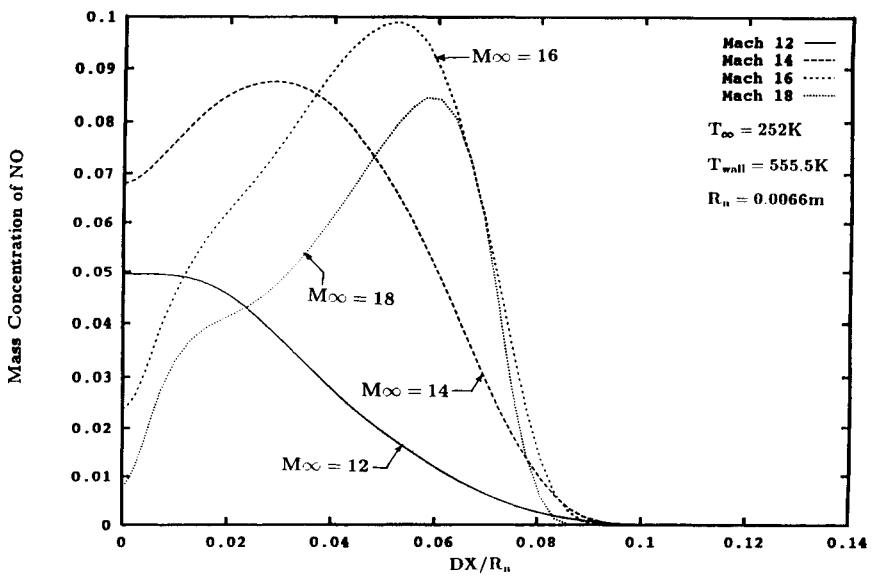

Fig. 17 Comparison of mass concentration of NO along stagnation streamline at different Mach numbers.

O concentration on the surface is less than 10% for the case of Mach 12, but higher than 20% for Mach 18. The concentration of N_2 has the greatest variation among all species. For the case of Mach 18, steep gradients exist both in the post-shock region and near the surface. The concentration of N is negligible for the case of Mach 12, while at Mach 18 it reaches a peak of nearly 10% at the edge of the boundary layer.

The formation of NO shown in Fig. 17 does not exhibit consistent behavior. On the surface it increases from 5% for Mach 12 to nearly 7% for Mach 14, then decreases to less than 3% for Mach 16 and further reduces to less than 1% for Mach 18. Nitric oxide concentration in the vicinity of shock wave is the highest (about 10%) for the case of Mach 16 followed by Mach 14 and 18, with almost negligible concentration for Mach 12.

Conclusions

The hypersonic flow past blunt bodies with thermal and chemical nonequilibrium were numerically simulated for flow past blunt bodies. The present results compared well with theoretical and experimental work for surface heat transfer and pressure distributions. The flow physics and the vibrational relaxation behavior for a range of Mach numbers was studied. Stagnation point heat transfer for solutions with vibrational nonequilibrium are 10–23% higher than solutions with vibrational equilibrium in the Mach number range of 12–18 at 37-km altitude. The importance of the high kinetic energy of the oncoming flow on the stagnation point heat transfer was noted. The present study substantiates that surface heat transfer is inversely proportional to nose-radius and altitude. The study also substantiates that the Mach number independence principle of ideal gas for the shock-standoff distance does not hold for the dissociating gas. It is also shown that for prediction of stagnation point heat transfer, the role of the multitemperature model is important. This model also proves important for predicting peak temperatures in the shock layer and the shock-standoff distance. Over the range of Mach numbers from 12 to 18, the vibrational relaxational time to attain thermal equilibrium of vibration-translation coupling in the vicinity of the shock is the highest for Mach 12, and its effect on temperature distributions and species concentrations is noticeable.

Further research is urgently needed in the formulation of a physically meaningful model for vibration-dissociation coupling and numerical algorithm development for nonequilibrium hypersonic flows.

References

[1]Bertin, J. J., Glowinski, R., and Periaux, J., *Hypersonics*, Vols. I and II, Birkhauser, Boston, MA, 1989.

[2]Josyula, E., and Shang, J. S., "Numerical Simulation of Nonequilibrium Hypersonic Flow with Adaptive Grid," AIAA Paper 90-1490, June 1990.

[3]Josyula, E., and Shang, J. S., "Numerical Study of Hypersonic Dissociated Flow past Blunt Bodies," *AIAA Journal*, Vol. 29, No. 5, 1990, pp. 704–711.

[4]Josyula, E., Gaitonde, D., and Shang, J. S., "Nonequilibrium Hypersonic Flow Solutions Using the Roe Flux Difference Split Scheme," AIAA Paper 91-1700, June 1991.

[5]Park, C., "On Convergence of Computation of Chemically Reacting Flows," AIAA Paper 85-0247, Jan. 1985.

[6]Candler, G., "On the Computation of Shock Shapes in Nonequilibrium Hypersonic Flows," AIAA Paper 89-0312, Jan. 1989.

[7]Park, C., "Assessment of Two-Temperature Kinetic Model for Dissociating and Weakly Ionizing Nitrogen," *Journal of Thermophysics and Heat Transfer*, Vol. 2, No. 1, 1988, pp. 8–16.

[8]Marrone, P. V., and Treanor, C. E., "Chemical Relaxation with Preferential Dissociation from Excited Vibrational Levels," *Physics of Fluids*, Vol. 6, No. 9, 1963, pp. 1215–1221.

[9]Jaffe, R. L., "Rate Constants for Chemical Reactions in High Temperature Nonequilibrium Air," *Thermophysical Aspects of Re-Entry Flows*, edited by J. N. Moss and C. D. Scott, Vol. 103, Progress in Astronautics and Aeronautics, AIAA, New York, 1985, pp. 123–151.

[10]Sharma, S. P., Huo, W. M., and Park, C., "The Rate Parameters for Coupled Vibration-Dissociation in a Generalized SSH Approximation," AIAA Paper 88-2714, June 1988.

[11]Flament, C., "Dissociation-Vibration Coupling Application to Hypersonic Nozzle Flows," *La Recherche Aerospatiale*, Nos. 1991–2, 1991, pp. 67–68.

[12]Park, C., "Assessment of Two-Temperature Kinetic Model for Ionizing Air," *Journal of Thermophysics and Heat Transfer*, Vol. 3, No. 3, 1989, pp. 233–244.

[13]Landau, L., and Teller, E., "Zur Theorie der Schalldispersion," *Physikalische Zeitschrift der Sowjetunion*, Vol. 10, No. 1, 1936, pp. 34–43.

[14]Millikan, R. C., and White, D. R., "Systematics of Vibrational Relaxation," *Journal of Chemical Physics*, Vol. 39, No. 12, 1963, pp. 3209–3213.

[15]Cambier, J. L., and Menees, G. P., "A Multi Temperature TVD Algorithm for Relaxing Hypersonic Flows," AIAA Paper 89-1971, June 1989.

[16]Vincenti, W. G., and Kruger, C. H., *Introduction to Physical Gas Dynamics*, Wiley, New York, 1965.

[17]Lee, J. H., "Basic Governing Equations for the Flight Regimes of Aeroassisted Orbital Transfer Vehicles," *Thermal Design of Aeroassisted Orbital Transfer Vehicles*, edited by H. F. Nelson, Vol. 96, Progress in Astronautics and Aeronautics, AIAA, New York, 1985, pp. 3–53.

[18]Blottner, F. G., Johnson, M., and Ellis, M., "Chemically Reacting Viscous Flow Program for Multicomponent Gas Mixtures," Sandia Lab., Rept. SC-RR-70-754, Albuquerque, NM, Dec. 1971.

[19]Wilke, C. R., "A Viscosity Equation for Gas Mixtures," *Journal of Chemical Physics*, Vol. 18, No. 4, 1950, p. 517.

[20]Bird, R. B., Stewart, W. E., and Lightfoot, E. N., *Transport Phenomena*, Wiley, New York, 1960.

[21]Roe, P. L., "Characteristic Based Schemes for the Euler Equations," *Annual Review of Fluid Mechanics*, Vol. 18, 1986, pp. 337–365.

[22]Van Leer, B., "Towards the Ultimate Conservation Difference Scheme V, a Second Order Sequel to Godunov's Method," *Journal of Computational Physics*, Vol. 32, No. 1, 1979, pp. 101–136.

[23]Yee, H. C., "Upwind and Symmetric Shock-Capturing Schemes," NASA TM-89464, May 1987.

[24]Walters, R. W., Cinnella, P., Slack, D. C., and Halt, D., "Characteristic-Based Algorithms for Flows in Thermo-Chemical Nonequilibrium," *AIAA Journal*, Vol. 30, No. 5, 1992, pp. 1304–1313.

[25]MacCormack, R., "Current Status of Numerical Solutions of the Navier-Stokes Equations," AIAA Paper 85-0032, Jan. 1985.

[26]Barr, D., "Reacting Gas Experimental Data in Low Density Flow; Task IV. Numerical Verification of the Experimental Data over the Models," Wright Lab., Rept. WL-TR-91-3095, Wright-Patterson AFB, OH, Jan. 1992.

[27]Cassady, P. E., and Lieberg, S. F., "Planar Laser Induced Fluorescence Measurements in Hypersonic Air Flowfields," AIAA Paper 91-1492, June 1991.

[28]Rose, P. H., and Stark, W. I., "Stagnation Point Heat Transfer Measurements in Dissociated Air," *Journal of the Aeronautical Sciences*, Vol. 25, No. 2, 1958, pp. 86–97.

[29]Polyakov, Yu, A., "Stagnation Point Heat-Transfer Studies with a Blunt Body in a Shock Tube," *Heat Transfer—Soviet Research*, Vol. 1, No. 2, 1969, pp. 8–14.

[30]Fay, J., and Riddell, F., "Theory of Stagnation Point Heat Transfer Rate in Dissociated Air," *Journal of the Aeronautical Sciences*, Vol. 25, No. 2, 1958, pp. 73–85.

[31]Hoffman, K. A., Siddiqui, M. S., and Chiang, S. T., "Difficulties Associated with the Heat Flux Computations of High Speed Flows by the Navier-Stokes Equations," AIAA Paper 91-1467, Jan. 1991.

[32]Cassady, P., Lieberg, D., Shelton, D., and Barr, D., "Reacting Gas Experimental Data in Low Density Flow; Task III. Model Flowfield Experimental Surveys," Wright Lab., Rept. WL-TR-91-3077, Wright-Patterson AFB, OH, Oct. 1991.

[33]Cassady, P., Barr, D., and Shelton, D., "Reacting Gas Experimental Data in Low Density Flow; Task V. Critical Evaluation of the Experiment," Wright Lab., Rept. WL-TR-91-3114, Wright-Patterson AFB, OH, Jan. 1992.

[34]Hayes, W., and Probstein, R., *Hypersonic Flow Theory*, Vol. 1, Academic Press, New York, 1959.

[35]Candler, G. V., "The Computation of Weakly Ionized Flows in Thermochemical Nonequilibrium," Ph.D. Dissertation, Stanford Univ., Stanford, CA, 1988.